Fuel 329 (2022) 125374

Contents lists available at ScienceDirect

Fuel

journal homepage: www.elsevier.com/locate/fuel

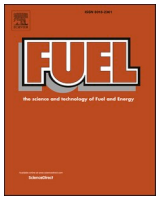

Full Length Article

The hysteresis of asphaltene-trapped saturated hydrocarbons during thermal evolution

Peng Fang [a,b], Jia Wu [a,b,*], Feng Chen [a], Yuan Wang [a,c], Xuan-Ce Wang [d], Keyu Liu [e], Minghui Zhou [f]

[a] State Key Laboratory of Petroleum Resources and Prospecting, China University of Petroleum (Beijing), Beijing 102249, China
[b] State Key Laboratory of Organic Geochemistry, Guangzhou Institute of Geochemistry, Chinese Academy of Sciences, Guangzhou 510640, China
[c] Wuxi Research Institute of Petroleum Geology, Petroleum Exploration and Production Research Institute, SINOPEC, Wuxi, Jiangsu 214216, China
[d] Research Centre for Earth System Science, Yunnan University, Kunming 650500, China
[e] School of Geosciences, China University of Petroleum (East China), Qingdao, Shandong 266580, China
[f] State Key Laboratory of Enhanced Oil and Gas Recovery, Research Institute of Petroleum Exploration and Development, PetroChina, Beijing 100083, China

ARTICLE INFO

Keywords:
Asphaltene
Adsorbed/Occluded hydrocarbon
Biomarker
Hysteresis
Thermal stability
Thermal evolution

ABSTRACT

Asphaltene-trapped (adsorbed or occluded) biomarkers are considered a valid source of information for crude oil with severe secondary alterations. However, thermal stress might change asphaltene-trapped hydrocarbons to some extent. Therefore, it is indispensable to investigate the thermal evolution behavior of asphaltene-trapped biomarkers. In this study, low-maturity bitumen from the Kuangshanliang area of the Sichuan Basin (China) was selected as a sample. The thermal evolution behavior of free and asphaltene-trapped saturated biomarkers was investigated by thermal simulation experiments. The results revealed, in addition to normal biomarkers, also a series of even carbon number *n*-alk-(1)-enes in asphaltene-occluded hydrocarbons. All of them were hardly influenced by secondary alterations. Moreover, due to the restriction of macromolecular structure, the thermal evolution of asphaltene-trapped biomarkers lags behind that of free biomarkers. Most biomarker parameters of occluded hydrocarbons changed little with increasing maturity. In particular, the distributions of occluded terpanes or steranes retained the characteristics of early diagenesis of organic matter, even if they suffered from strong thermal alteration.

1. Introduction

Asphaltenes, as "fragments" produced by thermal degradation of kerogen, are polar components of crude oil or source rock extracts with complex structures [1]. The structural model of asphaltenes assumes multistage aggregations, which are composed of polar monomers (islands or archipelagic molecules) [2–6]. Geogenic asphaltene aggregates tend to trap a series of autochthonous small molecular organics, including some common biomarkers, such as steranes and terpanes, through external side chain adsorption and internal space occlusion [7–10]. These asphaltene-trapped biomarkers are considered to be less susceptible to secondary alterations, thus maintaining superior autochthony Therefore, they have been used in applications of oil-source correlations, the assessment of source-rock sedimentary environments or the identification of biological origins [11–15].

Previously, adsorbed or occluded biomarkers in asphaltene were released by mild experimental procedures (such as stepwise elution or oxidative degradation) and then used to estimate the original geochemical information of sedimentary organic matter [16–19]. For instance, biomarkers trapped by the asphaltene matrix in some biodegradable oils lack the typical characteristics of biodegradation. This indicates that the asphaltene structure has a "shielding effect" against biodegradation. Therefore, the trapped biomarkers are useful to reveal raw information of oil biodegradation [17,20–22].

However, the "shielding effect" against biodegradation cannot prevent the influence of heating. Under geological conditions, asphaltene-trapped hydrocarbon molecules might be transformed to some extent due to thermal stress. Thus, it is indispensable to investigate the thermal evolution behavior of asphaltene-trapped biomarkers to provide the theoretical foundation for their applications [23–25].

Biomarkers occluded by kerogen matrix with high maturity showed better thermal stability than the adsorbed biomarkers [26,27]. It should

* Corresponding author at: State Key Laboratory of Petroleum Resources and Prospecting, China University of Petroleum (Beijing), Beijing 102249, China.
E-mail address: jia.wu@cup.edu.cn (J. Wu).

https://doi.org/10.1016/j.fuel.2022.125374
Received 11 April 2022; Received in revised form 9 July 2022; Accepted 20 July 2022

Table 1
Quantitative analysis of asphaltene-trapped hydrocarbons.

Components	T300		T350		T400	
	Weight (mg)	Yield (wt.%)	Weight (mg)	Yield (wt.%)	Weight (mg)	Yield (wt.%)
Purified Asphaltenes	30.5	/	30.6	/	30.3	/
Free Maltenes	0.4	1.3	1.4	4.6	2.9	9.6
Product Asphaltenes	20.3	66.6	15.5	50.7	3.0	9.9
Adsorbed Saturates	< 0.1	< 0.3	< 0.1	< 0.3	< 0.1	< 0.3
Occluded Saturates	0.4	1.3	0.3	1.0	0.2	0.7

Note: wt.% refers to the percentage of product *g* to the initial purified asphaltene *g*. The detection limit and the precision are 0.1 mg.

be noted that the chemical structure of kerogen will be destroyed during mild oxidative degradation [18,26], so it is impossible to guarantee that the distribution of the corresponding isolated occluded components remains unaffected. Due to the structural similarity of asphaltenes and kerogen, asphaltene-occluded biomarkers are expected to behave in the same way. Moreover, a nondestructive and quantitative approach may be used to isolate asphaltene-occluded biomarkers. Therefore, it is possible to reveal the thermal evolution behavior of occluded biomarkers if asphaltenes are treated as a macromolecular structure instead of kerogen.

In this study, low-maturity natural bitumen was selected as the experimental sample. Hydrous pyrolysis experiments in a closed system were conducted at 300 °C, 350 °C, and 400 °C. Centrifugal elution and dispersive solid-phase extraction (DSPE) were used to quantitatively and nondestructively isolate the trapped hydrocarbons of the asphaltene matrix after thermal simulation experiments [28,29]. The thermal evolution characteristics of typical biomarkers in different occurrences (free, adsorbed, and occluded) were systematically analyzed, and a corresponding mechanism of the evolution was also suggested.

2. Materials and methods

2.1. Sample information and pretreatment

The solid bitumen sample was collected from a Lower Cambrian bituminous vein from the Kuangshanliang area, northwestern Sichuan Basin, China. The bituminous vein may be derived from a paleo-reservoir, the source rock of which is the Sinian Doushantuo Formation. The paleo-reservoir has undergone tectonic transformations (e.g., uplift, fracture, fault) and subsequent secondary alterations (water washing, evaporation, biodegradation, abiotic oxidation) [30,31]. The equivalent vitrinite reflectance of the bitumen is approximately 0.55 %, revealing its low degree of thermal evolution. The bitumen is considered oxidized with enrichment of soluble organic matter (>90 wt%) [21,32].

The crushed bitumen sample (80 ~ 100 mesh) was extracted with dichloromethane (DCM). The maltene of the extract was obtained after asphaltene precipitation with an excess of petroleum ether. The saturated fraction (free saturates hereinafter) of maltene was eluted with petroleum ether in a silica gel alumina column. The asphaltene was dissolved in DCM to form an almost saturated solution, and then excessive petroleum ether was added. The mixture was stirred fully and then moved into a centrifuge tube for centrifugation treatment (3500 r/min, 20 min). The resulting supernatant was collected in a new beaker. The above protocol was repeated 3–5 times until the supernatant was colorless [12,13,21]. The collected supernatant was concentrated, and the corresponding saturated fraction (adsorbed saturates hereinafter) was isolated by the abovementioned approach. On the other hand, the asphaltene precipitate from the centrifugal tube was recovered and dried (purified asphaltene hereinafter).

2.2. Thermal simulation experiments

Hydrous pyrolysis was conducted with a gold-tube thermal simulation device [21]. Purified asphaltene (approximately 30 mg) and deionized water (approximately 100 mg) were successively loaded into a gold tube, which was sealed with Ar-arc welding. The experimental pressure was set as 30 MPa, and the temperatures were set as 300 °C, 350 °C, and 400 °C (marked as T300, T350, and T400). The rapid temperature rise method was adopted (all reaction vessels were heated to the set temperature within 1 h and kept at a constant temperature for 24 h). The corresponding EASY%R_o values were 0.64 %, 0.92 % and 1.49 %, respectively [33].

2.3. Separation of asphaltene-occluded hydrocarbons

The gold tubes were cut and then placed in petroleum ether to extract maltene from the products. Then, free saturates in maltene were separated by column chromatography as mentioned before. The asphaltenes in the residue were extracted by DCM and then purified by centrifugal elution. The adsorbed saturates were separated simultaneously.

Dispersive solid-phase extraction was used to separate the asphaltene-occluded hydrocarbons [29,54]. The purified asphaltenes were put in a beaker, and then an excess of DCM was added to it (the concentration was close to 0.1 mg/mL). The asphaltene solution was continuously stirred with a magnetic stirrer, and a small amount of silica gel (approximately 5 g) was added to it several times. After stirring for 30 min, the silica gel particles were rapidly precipitated by the centrifugal method. After centrifugation, the supernatant was separated by filtration. Then, the silica gel particles were cleaned 3–5 times with DCM, and the supernatant was separated as before. All filtrates were transferred to a flask and evaporated by rotation to concentrate to 2–3 mL. The saturates in concentrated solution were eluted with petroleum ether by column chromatography (called occluded saturates).

2.4. GC–MS analysis

The saturated hydrocarbons were analyzed on a 6890 GC − 5975i MS system (Agilent, USA) equipped with an HP-5MS fused-silica capillary chromatographic column (length, 60 m; inner diameter, 250 μm; film thickness, 0.25 μm). The injection method was a splitless inlet, and the temperature of the injection port was kept at 300 °C. Helium was used as a carrier gas with a constant flow rate of 1 mL/min. The column temperature was programmed as follows: 80 °C for 1 min, 80 °C to 120 °C at 20 °C/min, 120 °C for 1 min, 120 °C to 310 °C at 3 °C/min, and finally 310 °C for 20 min. In the MS system, the eluted products were fragmented by electron ionization (EI) at 70 eV and then analyzed in the *m/z* range of 50 to 450. Mass chromatograms were obtained by total ion current (TIC) recording and single ion monitoring (SIM) of characteristic fragment ions.

3. Results

Purified asphaltenes from the raw sample, which excluded free and adsorbed components, were used in thermal simulation experiments. Although the coking amount of the product increased and the soluble organic matter decreased with increasing thermal simulation temperature, a certain amount of asphaltenes and asphaltene-trapped saturates were still separated (Table 1).

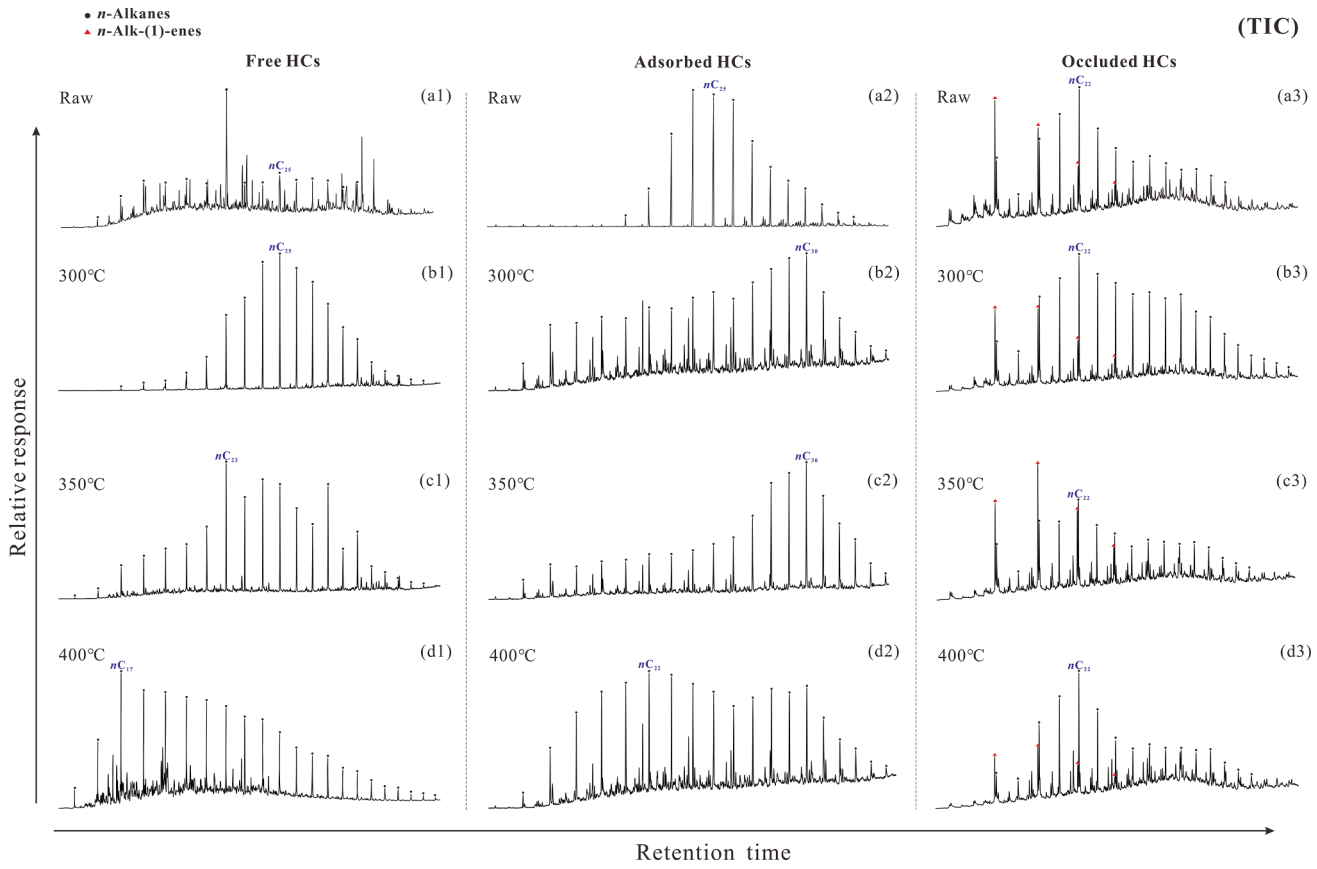

Fig. 1. Total ion current (TIC) chromatograms of the free, adsorbed, and occluded fractions of asphaltenes.

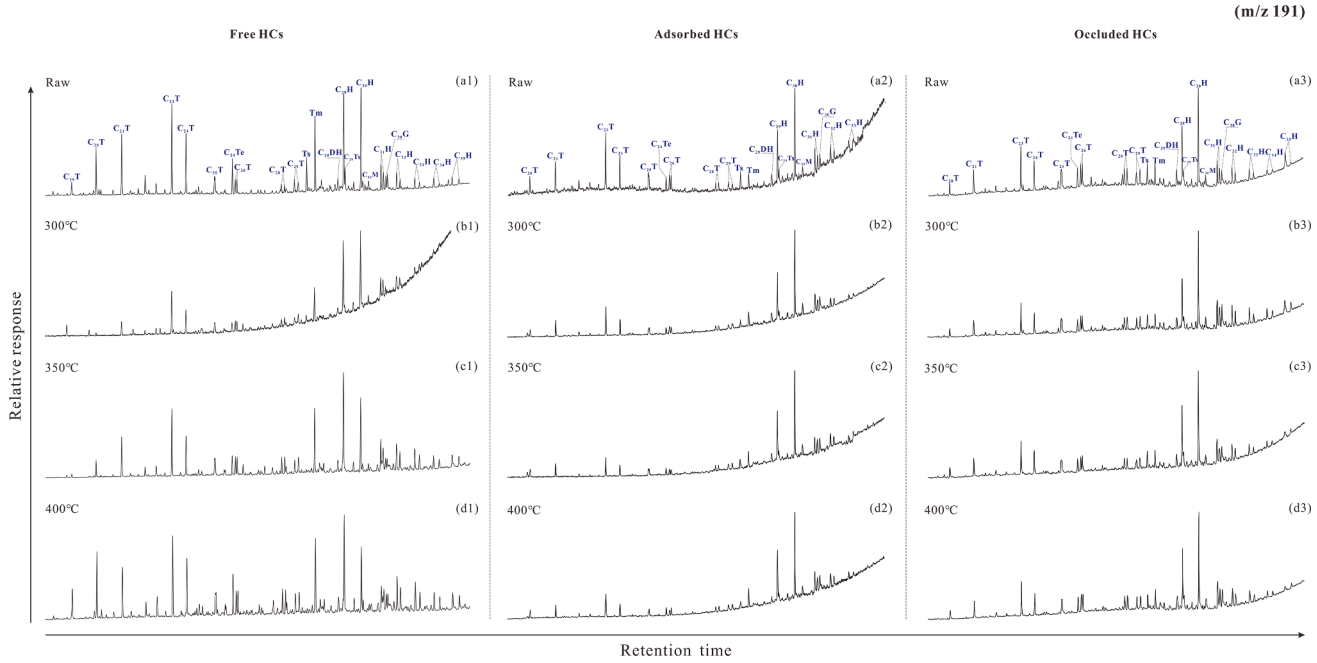

Fig. 2. Chromatograms of terpanes from free, adsorbed, and occluded fractions of asphaltenes. Biomarker assignments are listed in Table 2.

3.1. Distribution of n-alkanes and n-alkenes

Free hydrocarbons: Bitumen has undergone secondary alterations such as biodegradation, and most of the free *n*-alkanes have been damaged (Fig. 1a1). At 300 °C, the saturates exhibited a unimodal distribution of *n*-alkanes, with nC_{25} as the main peak (Fig. 1b1) [21]. The relative abundance of the low carbon number homologs of *n*-alkanes increased obviously with increasing temperature (Fig. 1c1 and d1).

Adsorbed hydrocarbons: The adsorbed *n*-alkanes of raw asphaltenes showed a unimodal distribution with nC_{24}, nC_{25}, and nC_{26} as the

Table 2
Compound assignments for the peaks in Fig. 2.

Class	Peak	Compound
Tricyclic terpanes	C_{20}T-C_{29}T	C_{20}-C_{26} tricyclic terpanes
Tetracyclic terpanes	C_{24}Te	C_{24} tetracyclic terpane
Pentacyclic terpenes	Ts	C_{27} 18α(H)–22,29,30-trisnorhopane
	Tm	C_{27} 17α(H)–22,29,30-trisnorhopane
	C_{29}DH	C_{29} 17α,21β(H)-25-norhopane
	C_{29}H	C_{29} 17α,21β(H)-30-norhopane
	C_{29}Ts	C_{29} 18α(H)-30-norneohopane
	C_{30}H	C_{30} 17α,21β(H)-hopane
	C_{30}M	C_{30} 17β,21α(H)-moretane
	C_{31}H-C_{35}H	C_{31}-C_{35} 17α,21β(H)-22S-and-22R-homohopane
	C_{30}G	gammacerane

main compounds (Fig. 1a2). At 300 °C and 350 °C, the main peak of *n*-alkanes moved to nC_{30} (Fig. 1b2 and c2). At 400 °C, the *n*-alkanes changed to the front high bimodal distribution (Fig. 1d2).

Occluded hydrocarbons: In raw asphaltene-occluded saturates, the *n*-alkanes ranged from $nC_{18} \sim nC_{30}$, and even carbon numbered *n*-(1)-alkenes ranged from $C_{18} \sim C_{24}$. (Fig. 1a3). Under different temperatures, *n*-alkanes always took nC_{22} as the main peak, and the abundance of $nC_{18} \sim nC_{25}$ was higher than that of $nC_{26} \sim nC_{30}$. Even carbon-numbered *n*-(1)-alkenes were distributed in $C_{18} \sim C_{24}$, with C_{18} and C_{20} as the dominant peaks (Fig. 1b3, c3, and d3).

3.2. Distribution of terpanes

Free hydrocarbons: The relative abundances of tricyclic terpanes and hopanes in raw asphaltenes were similar (Fig. 2a1). At 300 °C, the relative abundance of tricyclic terpanes was lower than that of hopanes (Fig. 2b1). The relative abundance of $C_{19}T \sim C_{25}T$ in terpanes increased obviously with increasing temperature (Fig. 2c1 and 2d1). At 400 °C, the relative abundance of tricyclic terpanes was equivalent to that of hopanes, and this distribution was similar to that of terpanes in the raw sample. However, their origins may be different. The former may be related to the cracking of asphaltenes or long-chain hopanes, while the latter may be related to the better resistance of tricyclic terpanes to biodegradation [34,35]. The values of Tm/C_{30}H and C_{29}H/C_{30}H increased with temperature, indicating that the side chain of C_{30}H was cracked (Fig. 2b1, c1, and d1).

Adsorbed/Occluded hydrocarbons: The relative abundance of tricyclic terpanes in adsorbed and occluded hydrocarbons from raw asphaltenes was lower than that of corresponding hopanes (Fig. 2a2 and a3). The distributions of adsorbed (Fig. 2b2, c2, and d2) and occluded terpanes (Fig. 2b3, c3, and d3) were similar at different temperatures, and some parameters (i.e., C_{29}Ts/C_{29}H, C_{29}H/C_{30}H, C_{31}H 22S/(22S + 22R)) were similar to the corresponding raw values (Table 3).

3.3. Distribution of steranes

Free hydrocarbons: The abundant short-chain pregnanes (C_{21}P and C_{22}P) and C_{29} steranes in the raw sample may be caused by biodegradation (Fig. 3a1) [19]. At 300 °C, the relative abundance of pregnanes in steranes was lower than that of normal steranes, and normal steranes still had a C_{29} advantage (Fig. 3b1). As the temperature advanced, the relative abundance of pregnanes gradually increased. This result was similar to the change in tricyclic terpanes mentioned in Section 3.2 (Fig. 3c1 and d1).

Adsorbed/Occluded hydrocarbons: The relative abundances of pregnanes and rearranged steranes in raw asphaltene-adsorbed steranes was obviously lower than those of normal steranes, and the series of C_{27}-C_{29} normal steranes were distributed in a "V" shape (Fig. 3a1). The relative abundance of pregnanes in occluded steranes was lower than that in adsorbed steranes, while the occluded rearranged steranes were slightly abundant. Occluded normal steranes had a C_{27} advantage (Fig. 3a3). At 300 °C, the distribution of adsorbed or occluded steranes was similar to that in the raw sample (Fig. 3b2 and b3). As the temperature advanced, the relative abundance of pregnanes in adsorbed steranes increased (Fig. 3c2 and d2), and the ratio of C_{21}P/C_{22}P increased obviously, while the other parameters were stable. The distribution characteristics of occluded steranes were relatively stable (Fig. 3c3 and d3), and only the ratio of C_{21}P/C_{22}P increased slightly as the temperature advanced (Table 5).

Table 4
Compound assignments for the peaks in Fig. 3.

Class	Peak		Compound
Pregnanes	C_{21}P		C_{21} 5α(H)-Pregnane
	C_{22}P		C_{22} 5α(H)-homopregnane
Rearranged steranes	C_{27}S	1	C_{27} 13β,17α(H)-rearranged sterane(20S)
		2	C_{27} 13β,17α(H)-rearranged sterane(20R)
		3	C_{27} 13α,17β(H)-rearranged sterane(20S)
	———	4	C_{27} 13α,17β(H)-rearranged sterane(20R)
	C_{28}S	5	C_{28} 13β,17α(H)-rearranged sterane(20S)
		6	C_{28} 13β,17α(H)-rearranged sterane(20R)
	C_{29}S	11	C_{29} 13β,17α(H)-rearranged sterane(20R)
		12	C_{29} 13α,17β(H)-rearranged sterane(20S)
Regular steranes	C_{27}S	7	C_{27} 5α,14α,17α(H)-sterane(20S)
		8	C_{27} 5α,14β,17β(H)-sterane(20R)
		9	C_{27} 5α,14β,17β(H)-sterane(20S)
		10	C_{27} 5α,14α,17α(H)-sterane(20R)
	C_{28}S	13	C_{28} 5α,14α,17α(H)-sterane(20S)
		14	C_{28} 5α,14β,17β(H)-sterane(20R)
		15	C_{28} 5α,14β,17β(H)-sterane(20S)
		16	C_{28} 5α,14α,17α(H)-sterane(20R)
	C_{29}S	17	C_{29} 5α,14α,17α(H)-sterane(20S)
		18	C_{29} 5α,14β,17β(H)-sterane(20R)
		19	C_{29} 5α,14β,17β(H)-sterane(20S)
		20	C_{29} 5α,14α,17α(H)-sterane(20R)

Table 3
Terpane parameters of free, adsorbed, and occluded Saturates in Asphaltenes.

Components	Temperature	Tri/Pentacyclic terpene	Ts/Tm	C_{29}Ts/C_{29}H	C_{29}H/C_{30}H	C_{29}DH/C_{30}H	C_{30}M/C_{30}H	C_{30}G/C_{30}H	C_{31}H 22S/(22S + 22R)
Free Hydrocarbons (HCs)	Raw	1.24	0.45	0.25	1.02	0.15	0.10	0.17	0.57
	300 °C	0.52	0.27	0.13	0.93	0.15	0.11	0.15	0.55
	350 °C	0.83	0.05	0.06	1.47	0.21	0.12	0.22	0.53
	400 °C	1.40	0.06	0.05	1.62	0.32	0.13	0.29	0.52
Adsorbed Hydrocarbons (HCs)	Raw	0.91	1.08	0.27	0.58	0.17	0.15	0.26	0.54
	300 °C	0.49	0.65	0.29	0.52	0.12	0.18	0.26	0.56
	350 °C	0.39	0.61	0.22	0.59	0.14	0.16	0.25	0.54
	400 °C	0.42	0.54	0.23	0.60	0.16	0.17	0.25	0.55
Occluded Hydrocarbons (HCs)	Raw	0.69	1.01	0.32	0.66	0.23	0.13	0.18	0.54
	300 °C	0.54	0.89	0.37	0.57	0.18	0.14	0.30	0.56
	350 °C	0.57	0.90	0.37	0.61	0.17	0.16	0.24	0.54
	400 °C	0.54	0.79	0.33	0.67	0.21	0.16	0.23	0.54

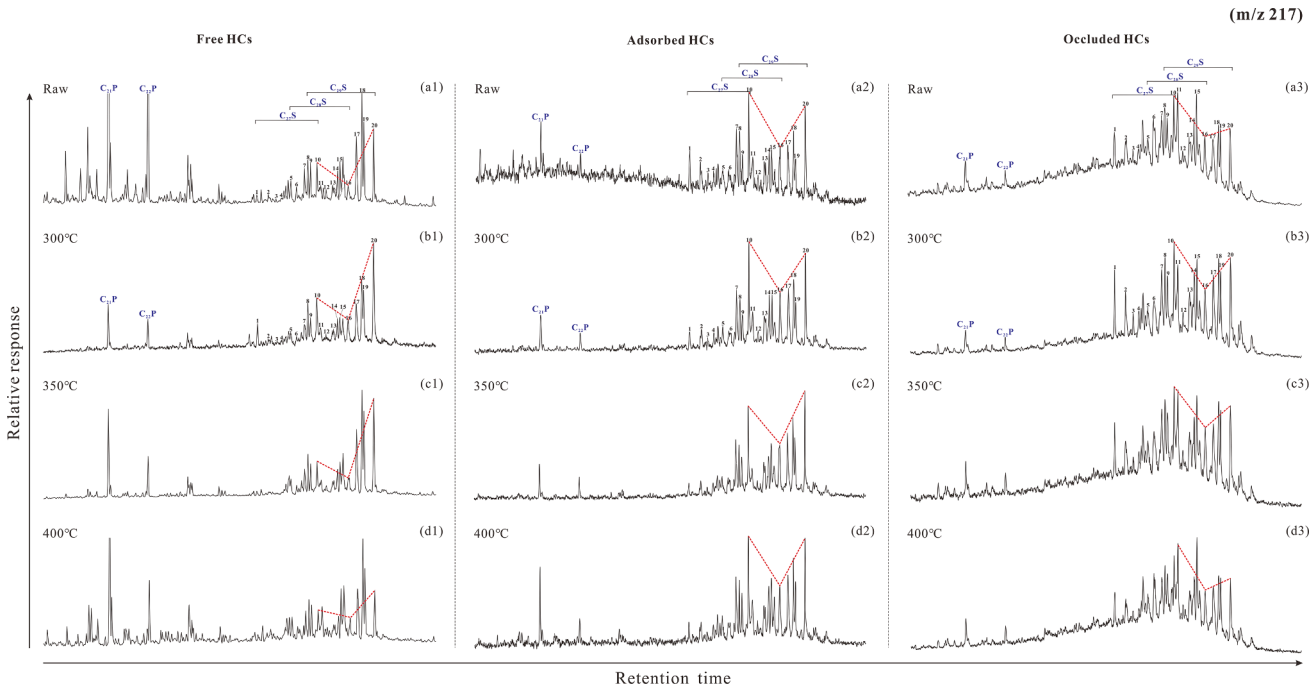

Fig. 3. Chromatograms of steranes from free, adsorbed, and occluded fractions of asphaltenes. Biomarker assignments are listed in Table 4.

Table 5
Sterane parameters in free, adsorbed, and occluded Saturates of Asphaltenes.

Components	Temperature	$C_{21}P/C_{22}P$	$C_{21}-C_{22}P/C_{27}-C_{29}S$	$C_{27}S/C_{27}-C_{29}S$	$C_{28}S/C_{27}-C_{29}S$	$C_{29}S/C_{27}-C_{29}S$	$C_{29}S\alpha\alpha\alpha$ 20S/(20S + 20R)	$C_{29}S\alpha\beta\beta/(\alpha\alpha\alpha + \alpha\beta\beta)$	Rearranged/Regular sterane
Free	Raw	2.30	1.14	0.22	0.21	0.57	0.54	0.53	0.15
HCs	300 °C	1.49	0.13	0.27	0.19	0.54	0.34	0.43	0.18
	350 °C	2.25	0.20	0.20	0.18	0.62	0.46	0.50	0.17
	400 °C	3.78	0.48	0.24	0.23	0.52	0.58	0.55	0.22
Adsorbed	Raw	1.52	0.06	0.37	0.30	0.33	0.45	0.38	0.31
HCs	300 °C	1.57	0.07	0.32	0.29	0.39	0.46	0.40	0.25
	350 °C	1.78	0.08	0.29	0.28	0.43	0.46	0.42	0.20
	400 °C	2.85	0.12	0.33	0.29	0.38	0.47	0.41	0.23
Occluded	Raw	1.37	0.08	0.32	0.34	0.34	0.48	0.42	0.50
HCs	300 °C	1.39	0.05	0.36	0.26	0.38	0.46	0.40	0.40
	350 °C	1.58	0.08	0.31	0.28	0.41	0.47	0.42	0.36
	400 °C	1.72	0.06	0.34	0.30	0.36	0.49	0.45	0.37

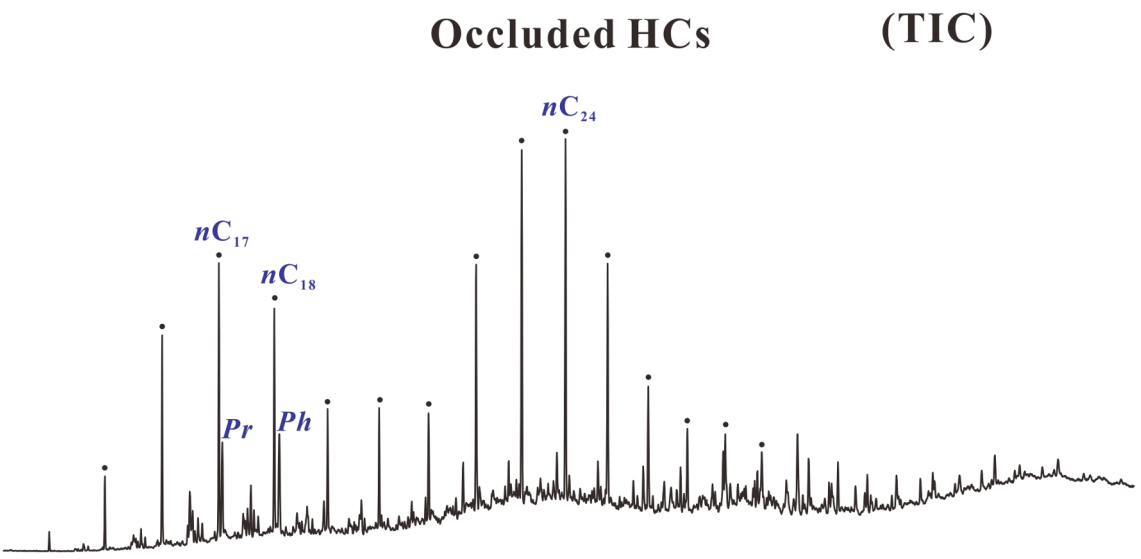

Fig. 4. Asphaltenes occluded saturates exposed to air for more than four days.

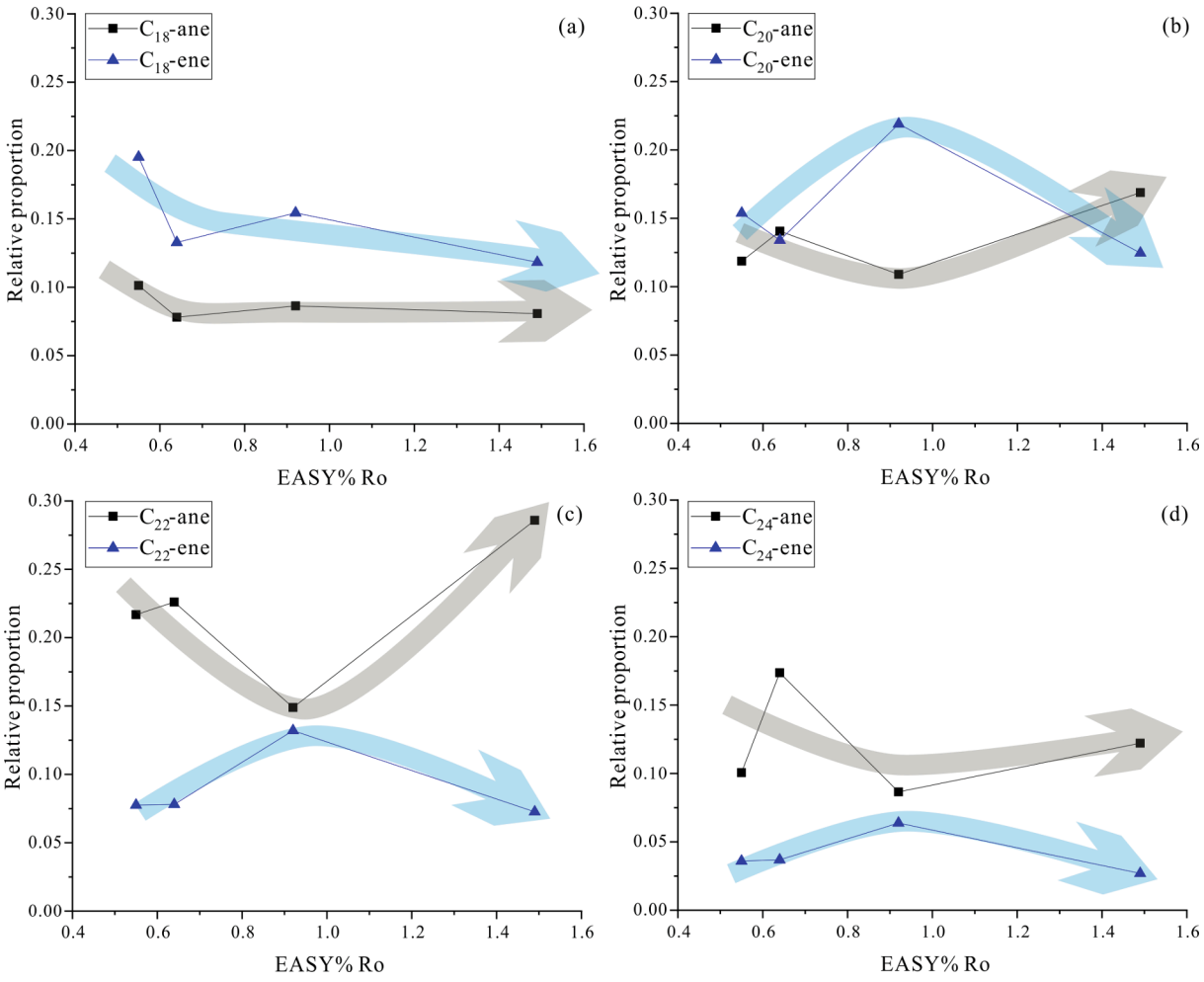

Fig. 5. Variation in the relative proportion of occluded *n*-alkenes and *n*-alkanes from C_{18}-C_{24} with EASY%R_o.

4. Discussion

4.1. Thermal evolution of asphaltene-trapped n-alkenes and n-alkanes

At 300 °C and 350 °C, the relative abundance of low carbon numbered *n*-alkanes (nC_{17} ~ nC_{25}) was inferior in adsorbed *n*-alkanes (Fig. 1b2 and c2). This was similar to that of free *n*-alkanes (Fig. 1b1 and c1). However, the relative abundance of adsorbed *n*-alkanes with high carbon numbers (nC_{26} ~ nC_{32}) was greater than that with low carbon numbers, which was different from the distribution of free *n*-alkanes. Because asphaltene only cracks very slightly at 300 °C or 350 °C [36,37], the pyrolytic free *n*-alkanes were probably derived from the thermal diffusion of the hydrocarbons trapped in the level of the asphaltene cluster, and the residue of diffusion may constitute pyrolytic adsorbed *n*-alkanes [21].

At 400 °C, the relative abundance of low carbon numbered *n*-alkanes adsorbed by asphaltenes increased significantly (Fig. 1d2). The intensity ratio between nC_{22} and nC_{30} is over 1, indicating the cracking of long-chain hydrocarbons. In contrast, the relative abundance of short-chain alkanes in free *n*-alkanes was higher (Fig. 1d1), indicating the high cracking extent of long-chain hydrocarbons. Therefore, the profile of adsorbed *n*-alkanes was less affected by thermal cracking than that of free *n*-alkanes.

Even carbon numbered *n*-(1)-alkenes were obviously present in the occluded hydrocarbons separated from the raw asphaltene sample (Fig. 1a3) [14,27]. Similar *n*-(1)-alkenes are often observed in separation experiments of asphaltene from crude oil [9]. Importantly, the even carbon numbered *n*-(1)-alkenes occluded by asphaltene were still preserved well after the thermal simulation experiments (Fig. 1b3, c3, and d3). As small molecules with high chemical activity, once separated from asphaltene, alkenes are easily affected by the external environment. For example, it is almost impossible to detect alkenes in the occluded saturates exposed to air for more than four days (Fig. 4). However, the relative profiles of *n*-(1)-alkenes with different carbon numbers after heating were generally consistent with that of the raw sample. This suggests that asphaltene-occluded alkenes could be quite stable under geological conditions.

The proportion of nC_{20} ~ nC_{24} alkanes in occluded saturates rose at the beginning and then fell with the increase in EASY%R_o, whereas the proportion of individual *n*-alkenes changed in the opposite way (Fig. 5). This indicates that the variations in *n*-alkanes and *n*-alkenes from C_{20} ~ C_{24} were coupled. This could be attributed to the closed space constituted by the asphaltene matrix, which provided the environmental foundation for the chemical conversion between alkanes and alkenes [14]. The proportion of C_{18} alkanes and alkenes generally showed a slight downward trend with the variation in EASY%R_o, and the decline in C_{18} alkenes was slightly larger (Fig. 5a). We speculated that both C_{18} alkanes and alkenes were consumed in other ways.

In theory, the conversion between alkanes and alkenes occluded in asphaltene structures is thermodynamically constrained under hydrothermal conditions [38,39]. Thus, it could reach a metastable equilibrium at a given temperature [40,41]. It should be noted that the tendency of the conversion between alkenes and alkanes in this study could be divided into two stages (Fig. 5b, c, and d). This indicates some

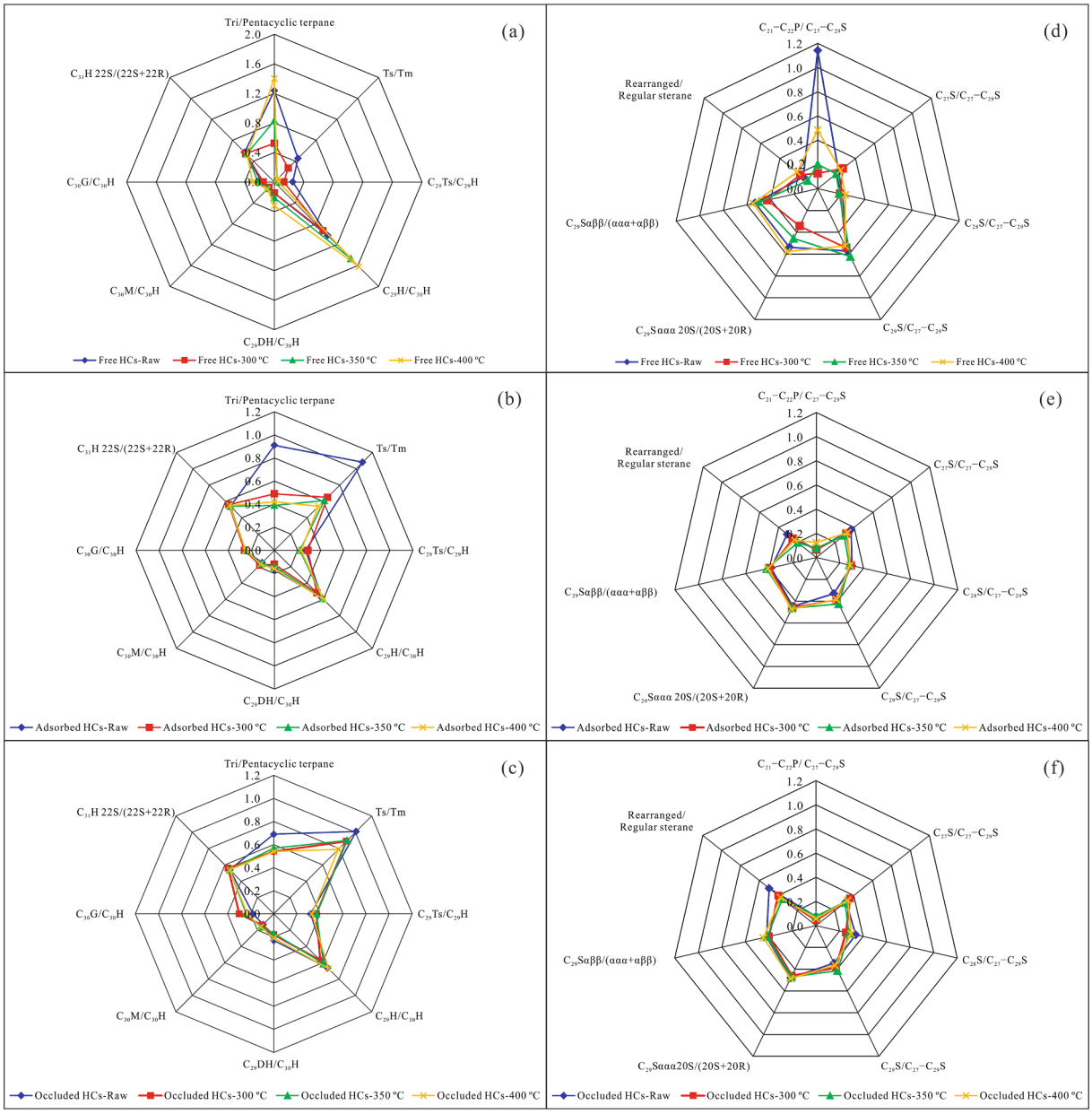

Fig. 6. Fingerprint of free, adsorbed, and occluded biomarker parameters (a-c: Free, adsorbed, and occluded terpane parameters; d-f: Free, adsorbed, and occluded sterane parameters).

other factors restricting the metastable equilibrium between alkenes and alkanes.

The hydrogen fugacity controlled by redox mineral buffers has been proven to be an important geological factor for the metastable equilibrium of short alkene-alkane [41]. The equivalent hydrogen fugacity in the experimental system was determined by the rate of generation and consumption with the sedimentary organic matter, so it is related to the chemical property of asphaltene and the corresponding extent of thermal evolution. Therefore, it is also reasonable to conclude that the metastable equilibrium of alkene-alkane in the asphaltene structure can be influenced by the equivalent hydrogen fugacity.

4.2. Persistence of asphaltene-trapped terpanes and steranes

The ratios of Tri/Pentacyclic terpane, Ts/Tm, $C_{29}Ts/C_{29}H$, $C_{29}H/C_{30}H$, and $C_{29}DH/C_{30}H$ in free terpanes changed obviously with temperature (Fig. 6a), while the ratios of $C_{30}M/C_{30}H$, $C_{30}G/C_{30}H$, and $C_{31}H$ 22S/(22S + 22R) were almost consistent. For example, the ratio of $C_{31}H$ 22S/(22S + 22R) is approximately 0.55 and cannot be used to indicate maturity [19,42]. On the other hand, most of the parameters of adsorbed/occluded terpanes did not change with temperature, suggesting that the trapped terpanes might remain authentic and not be altered by asphaltene cracking (Fig. 6b and c).

The trapped hydrocarbons on the periphery of the asphaltene cluster, defined as adsorbed hydrocarbons, were isolated by centrifugation. However, there are some components trapped in the inner layers of the asphaltene cluster. The corresponding position is different from that of the occluded ones, which are trapped in the asphaltene nanoaggregate. The former could diffuse outside during heating, and it would produce pyrolytic free or adsorbed hydrocarbons [21]. This probably results in a small discrepancy between the raw trapped biomarkers and the pyrolytic ones. For example, the ratios of Tri/Pentacyclic terpane and Ts/Tm in the raw adsorbed terpanes were obviously higher than those of the adsorbed hydrocarbons in the pyrolytic products [8,43,44]. In addition,

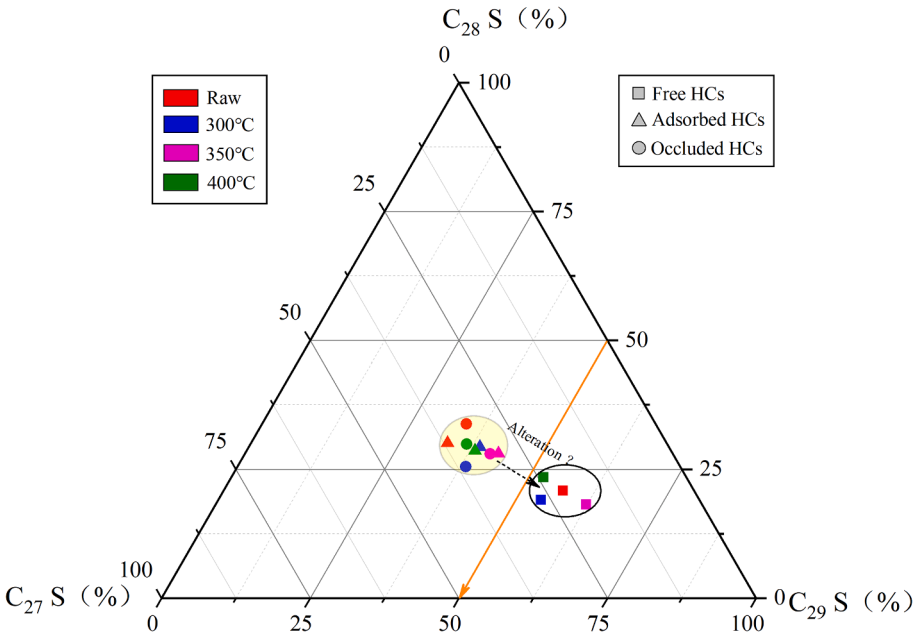

Fig. 7. C_{27}–C_{29} regular sterane distribution.

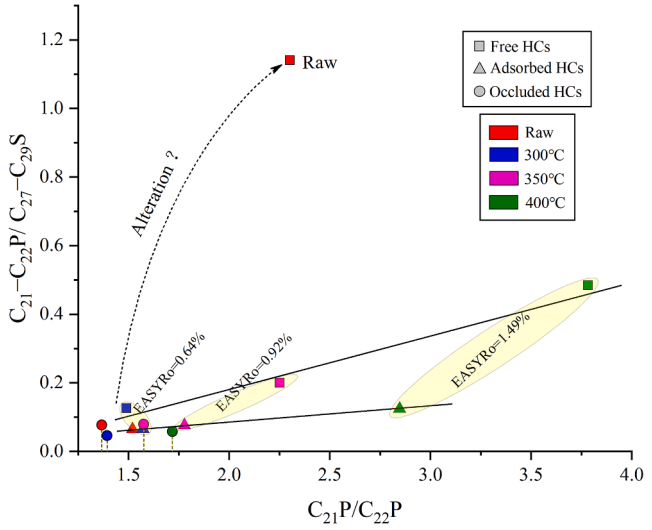

Fig. 8. Intersection figure of $C_{21}P/C_{22}P$ and $C_{21}-C_{22}P/C_{27}-C_{29}S$.

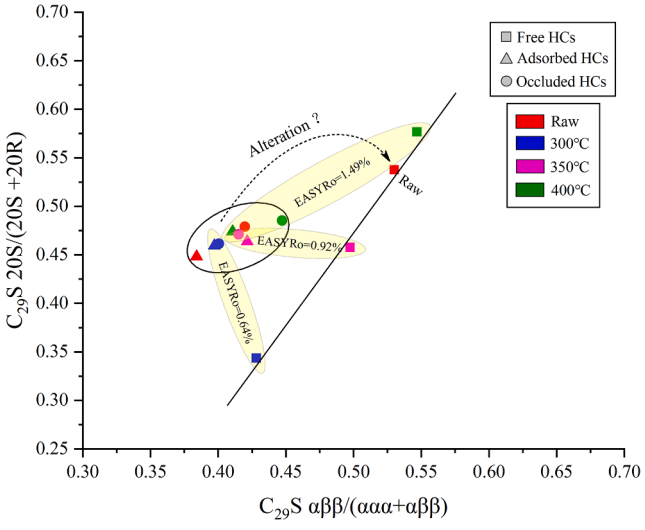

Fig. 9. Intersection figure of $C_{29}S\alpha\alpha\alpha$ 20S/(20S + 20R) and $C_{29}S\alpha\beta\beta/(\alpha\alpha\alpha + \alpha\beta\beta)$.

the ratios of Tri/Pentacyclic terpane and Ts/Tm in the occluded terpanes of the raw asphaltene were slightly higher than those in occluded biomarkers of the pyrolytic products. Except for the fact that the raw free steranes were affected by secondary alterations, most parameters of free steranes also changed with temperature, whereas the parameters of adsorbed or occluded steranes were almost always consistent (Fig. 6d-f).

The biomarker parameters of asphaltene-occluded steranes and terpanes were affected by neither secondary changes nor potential fractionation caused by different separation protocols. The occluded compounds are restricted by the macromolecular structure of asphaltene during pyrolysis and rarely suffer thermal cracking. Moreover, the pyrolytic substances of asphaltene would be released and gather in a free state, which hardly changes the distribution characteristics of the occluded hydrocarbons. Therefore, the profiles of asphaltene-occluded biomarkers are probably consistent during the evolution of crude oil, and they have the potential to trace the biological source and sedimentary environment of organic matter [45,46].

4.3. *Geochemical significance of asphaltene-trapped biomarkers*

The bitumen sample comes from the Sinian paleo-reservoir, and its source rock is generally considered the Sinian Doushantuo Formation. The biological source of sedimentary organic matter in the Doushantuo Formation is lower aquatic plankton such as algae. Its typical biomarkers display similar distribution characteristics to those of asphaltene-occluded *n*-alkanes [34].

The values of adsorbed and occluded sterane proportions both fell in the same area of the ternary diagram, but those of free steranes were close to the end of $C_{29}S$ (Fig. 7). Although the contribution of lower aquatic plankton, such as cyanobacteria, may produce a $C_{29}S$ advantage, biodegradation can easily change the distribution of free steranes, resulting in the predominance of $C_{29}S$ [19,30].

According to our study, the values of occluded sterane proportions are more primitive with the reflection of authentic geochemical information. Therefore, the occluded steranes may be related to the

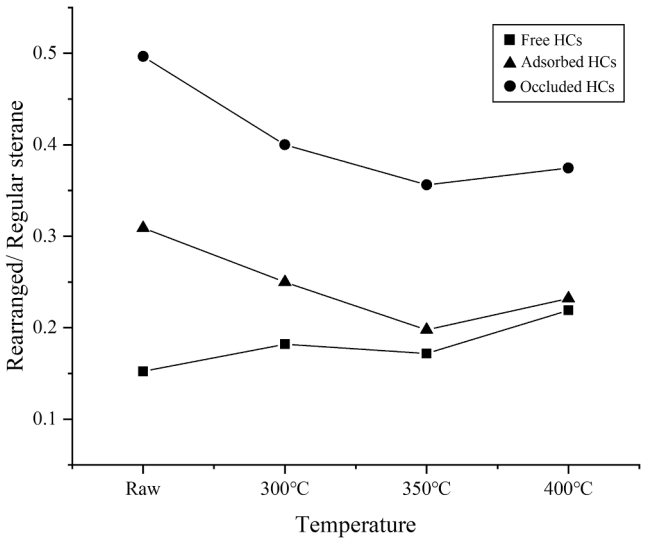

Fig. 10. Diagram of Rearranged/Regular steranes with temperature.

eukaryotic algae of the Precambrian rather than cyanobacteria, resulting in the distribution of steranes not being dominated by $C_{29}S$ [47,48].

The increments of $C_{21}P/C_{22}P$ and $C_{21}-C_{22}P/C_{27}-C_{29}S$ in adsorbed steranes were less than those in free steranes with increasing thermal maturation (Fig. 8). The corresponding parameters of free sterane in the raw sample obviously deviate, which may be related to the secondary alterations of bitumen [19,34]. The values of $C_{21}P/C_{22}P$ in occluded steranes increased slightly with thermal maturation, and the values of $C_{21}-C_{22}P/C_{27}-C_{29}S$ were constant.

The values of $C_{29}S\alpha\alpha\alpha20S/(20S + 20R)$ and $C_{29}S\alpha\beta\beta/(\alpha\alpha\alpha + \alpha\beta\beta)$ of the adsorbed and occluded steranes in all samples are similar. This result is consistent with the original characteristics of low maturity, with the corresponding values of that area being stable at 0.4 ~ 0.5 (not reaching the equilibrium value) [32]. However, the values of the two parameters of the free steranes increased significantly with maturation (Fig. 9). Therefore, the maturity parameters of steranes in asphaltene-trapped hydrocarbons are independent of maturation.

Generally, the ratio of Rearranged/Regular steranes generally increases with thermal maturation or biodegradation [42]. The raw bitumen suffered from biodegradation. However, the ratio of Rearranged/Regular steranes in raw occluded hydrocarbons was greater than that in raw free ones (Fig. 10). In the early stage of diagenesis, steranes are generated from the reduction of the precursors in the sediments. This process is followed by isomerization and rearrangement to form rearranged steranes [49].

The presence of free oxygen would accelerate the acid catalytic rearrangement process of sterene in the early stage of diagenesis, while this process would be inhibited in the absence of oxygen [50–53]. The rearranged steranes were probably trapped in the asphaltene structure during diagenesis. As the free oxygen in the environment was exhausted, a more reduced condition at the beginning of catagenesis would lead to a decrease in rearranged steranes in free hydrocarbons. Thus, the ratio of Rearranged/Regular steranes in free hydrocarbons of the raw sample is lower than that in trapped hydrocarbons.

On the other hand, the ratios of Rearranged/Regular steranes in the free steranes of the experimental product increased as the maturity advanced because the free regular steranes undergo the reaction of methyl rearrangement [42]. However, the ratios of Rearranged/Regular steranes in trapped hydrocarbons fell at the beginning and then rose with thermal maturation (Fig. 10). Since the trapped steranes were less influenced by heating below 350 °C, the decrease in the ratios may result from the transformation of the trapped precursors into regular steranes. The methyl rearrangement of regular steranes gradually occurred with temperatures over 350 °C, increasing the ratios of Rearranged/Regular steranes.

5. Conclusion

There are significant discrepancies in the distribution characteristics of biomarkers in the three occurrence states of bitumen. The original characteristics of free hydrocarbons missed due to secondary alterations, so it is impossible to accurately evaluate the sedimentary environment and the biological source of organic matter. Adsorbed hydrocarbons and occluded hydrocarbons in asphaltenes were preserved well based on the restriction of the asphaltene structure. The distribution characteristics of occluded sterane or terpane are of great significance for tracing the original source of the sample.

The thermal evolution of occluded hydrocarbons obviously lags that of adsorbed and free hydrocarbons. The free and adsorbed *n*-alkanes are obviously affected by cracking products with increasing maturation. Occluded *n*-alkanes and *n*-alkenes can maintain relatively stable profiles during thermal evolution. The potential conversion between alkanes and alkenes is probably related to the equivalent hydrogen fugacity in the system.

The values of $C_{21}P/C_{22}P$, $C_{21}-C_{22}P/C_{27}-C_{29}S$, $C_{29}S\alpha\alpha\alpha20S/(20S + 20R)$, and $C_{29}S\alpha\beta\beta/(\alpha\alpha\alpha + \alpha\beta\beta)$ in free hydrocarbons are sensitive to maturation, whereas those of $C_{21}P/C_{22}P$ and $C_{21}-C_{22}P/C_{27}-C_{29}S$ in adsorbed hydrocarbons are less sensitive. The protection of the asphaltene matrix results in occluded biomarkers maintaining the characteristics of organic matter in diagenesis.

CRediT authorship contribution statement

Peng Fang: Methodology, Formal analysis, Investigation, Writing – original draft. **Jia Wu:** Conceptualization, Methodology, Writing – review & editing, Supervision, Funding acquisition. **Feng Chen:** Investigation. **Yuan Wang:** Investigation. **Xuan-Ce Wang:** Resources, Writing – review & editing, Supervision. **Keyu Liu:** Resources, Writing – review & editing. **Minghui Zhou:** Resources, Formal analysis.

Declaration of Competing Interest

The authors declare that they have no known competing financial interests or personal relationships that could have appeared to influence the work reported in this paper.

Data availability

The data that has been used is confidential.

Acknowledgment

We would like to thank Shengbao Shi, Lei Zhu, and Shuo Gao for their help with the organic geochemical experiments. Stephen R. Larter is thanked for his help in promoting the process of this study. This paper was supported by a grant from the State Key Laboratory of Petroleum Resources and Prospecting, China University of Petroleum (Beijing) (Grant No. PRP/indep-3-1715), and the State Key Laboratory of Organic Geochemistry, GIGCAS (Grant No. SKLOG202123).

References

[1] Bandurski E. Structural similarities between oil-generating kerogens and petroleum asphaltenes. Energy Sources 1982;6(1–2):47–66. https://doi.org/10.1080/00908318208946021.
[2] Evdokimov IN, Fesan AA. Multi-step formation of asphaltene colloids in dilute solutions. Colloids Surf, A 2016;492:170–80.
[3] Mullins OC, Sabbah H, Eyssautier J, Pomerantz AE, Barré L, Andrews AB, et al. Advances in asphaltene science and the Yen-Mullins model. Energy Fuels 2012;26(7):3986–4003.

[4] Rashid Z, Wilfred CD, Gnanasundaram N, Arunagiri A, Murugesan T. A comprehensive review on the recent advances on the petroleum asphaltene aggregation. J Pet Sci Eng 2019;176:249–68.
[5] Zuo P, Qu S, Shen W. Asphaltenes: separations, structural analysis and applications. J Energy Chem 2019;34(7):186–207.
[6] Siddiqui MN, Ali MF. Investigation of chemical transformations by NMR and GPC during the laboratory aging of Arabian asphalt. Fuel 1999;78(12):1407–16.
[7] Gray MR, Tykwinski RR, Stryker JM, Tan X. Supramolecular assembly model for aggregation of petroleum asphaltenes. Energy Fuels 2011;25(7):3125–34.
[8] Snowdon LR, Volkman JK, Zhang Z, Tao G, Liu P. The organic geochemistry of asphaltenes and occluded biomarkers. Org Geochem 2016;91:3–15.
[9] Yang C, Liao Z, Zhang L, Creux P. Some biogenic-related compounds occluded inside asphaltene aggregates. Energy Fuels 2009;23(1):820–7.
[10] Scott DE, Schulze M, Stryker JM, Tykwinski RR. Deciphering structure and aggregation in asphaltenes: hypothesis-driven design and development of synthetic model compounds. Chem Soc Rev 2021;50(16):9202–39.
[11] Liao Z, Zhou H, Graciaa A, Chrostowska A, Creux P, Geng A. Adsorption/occlusion characteristics of asphaltenes: some implication for asphaltene structural features. Energy Fuels 2005;19(1):180–6.
[12] Liao Z, Geng A, Graciaa A, Creux P, Chrostowska A, Zhang Y. Different adsorption/occlusion properties of asphaltenes associated with their secondary evolution processes in oil reservoirs. Energy Fuels 2006;20(3):1131–6.
[13] Liao Z, Geng A, Graciaa A, Creux P, Chrostowska A, Zhang Y. Saturated hydrocarbons occluded inside asphaltene structures and their geochemical significance, as exemplified by two Venezuelan oils. Org Geochem 2006;37(3):291–303.
[14] Cheng B, Zhao J, Yang C, Tian Y, Liao Z. Geochemical evolution of occluded hydrocarbons inside geomacromolecules: a review. Energy Fuels 2017;31(9):8823–32.
[15] Tian Y, Zhao J, Yang C, Liao Z, Zhang L, Zhang H. Multiple-sourced features of marine oils in the Tarim Basin, NW China – Geochemical evidence from occluded hydrocarbons inside asphaltenes. J Asian Earth 2012;54–55:174–81.
[16] Liao Z, Geng A. Characterization of nC7-soluble fractions of the products from mild oxidation of asphaltenes. Org Geochem 2002;33(12):1477–86.
[17] Pan C, Geng A, Liao Z, Xiong Y, Fu J, Sheng G. Geochemical characterization of free versus asphaltene-sorbed hydrocarbons in crude oils: implications for migration-related compositional fractionations. Mar Pet Geol 2002;19(5):619–32.
[18] Zhao J, Liao Z, Zhang L, Creux P, Yang C, Chrostowska A, et al. Comparative studies on compounds occluded inside asphaltenes hierarchically released by increasing amounts of H_2O_2/CH_3COOH. Appl Geochem 2010;25(9):1330–8.
[19] Fang P, Wu J, Li B, Wang X, Zhong N. Comparison of separation of asphaltene adsorbed hydrocarbons by different elution methods. Acta Pet Sin 2021;42(5):623–33. in Chinese.
[20] Ma A, Zhang S, Zhang D. Ruthenium-ion-catalyzed oxidation of asphaltenes of heavy oils in Lunnan and Tahe oilfields in Tarim Basin. NW China Org Geochem 2008;39(11):1502–11.
[21] Wu J, Fang P, Wang X-C, Li B, Liu K, Ma X, et al. The potential occurrence modes of hydrocarbons in asphaltene matrix and its geochemical implications. Fuel 2020;278:118233.
[22] Orea M, López L, Ranaudo MA, Faraco AK. Saturated biomarkers adsorbed and occluded by the asphaltenes of some Venezuelan crude oils: limitations in geochemical assessment and interpretations. J Pet Sci Eng 2021;206:109048.
[23] Connan J, Le Tran K, Van Der Weide B, editors. Tokyo, Japan: 2, Publisher; 1975. p. 171–8.
[24] Liao Y, Liu W, Pan Y, Wang X, Wang Y, Peng P. Superimposed secondary alteration of oil reservoirs. Part I: influence of biodegradation on the gas generation behavior of crude oils. Org Geochem 2020;142:103965.
[25] Liu W, Liao Y, Jiang C, Pan Y, Huang Y, Wang X, et al. Superimposed secondary alteration of oil reservoirs. Part II: the characteristics of biomarkers under the superimposed influences of biodegradation and thermal alteration. Fuel 2022;307:121721.
[26] Cheng B, Du J, Tian Y, Liu H, Liao Z. Thermal evolution of adsorbed/occluded hydrocarbons inside kerogens and its significance as exemplified by one low-matured kerogen from Santanghu basin, Northwest China. Energy Fuels 2016;30(6):4529–36.
[27] Cheng B, Yang CP, Du JY, Zhao J, Liao ZW. Determination of the series of even carbon numbered n-alk-1-enes trapped inside geomacromolecules. Mar Pet Geol 2014;51:49–51.
[28] Chisvert A, Cárdenas S, Lucena R. Dispersive micro-solid phase extraction. TrAC, Trends Anal Chem 2019;112:226–33.
[29] Fang P., Wu J., Li B., Qi W., Li M., Zhong N. Method for separating small molecular hydrocarbon coprecipitated with asphaltene: China, CN111205882B. 2021-03-16 (in Chinese).
[30] Wang G, Han K, Wang L, Shi S. Organic geochemical characteristics and origin of solid bitumen and oil sands in northwestern Sichuan. Pet Geol Exp 2014;36(6):731–5. in Chinese.
[31] Charrié-Duhaut A, Lemoine S, Adam P, Connan J, Albrecht P. Abiotic oxidation of petroleum bitumens under natural conditions. Org Geochem 2000;31(10):977–1003.
[32] Liang T, Zhan Z-W, Gao Y, Wang Y-P, Zou Y-R, Peng P. Molecular structure and origin of solid bitumen from northern Sichuan Basin. Mar Pet Geol 2020;122:104654.
[33] Sweeney J, Burnham A. Evaluation of a simple model of vitrinite reflectance based on Chemical kinetics. Aapg Bulletin - AAPG BULL 1990;74:1559–70.
[34] Cheng B, Hu SZ, Shen CB, Liao ZW, Liu H, Du JY, et al. The geochemical characterization of adsorbed/occluded hydrocarbons inside solid bitumen in the Kuangshanliang Area of the Northwestern Sichuan Basin and its significance. Pet Sci Technol 2014;32(18):2203–11.
[35] Zhang X, Shen B, Yang J, Sun W, Hou D. Evolution characteristics of maturity-related sterane and terpane biomarker parameters during hydrothermal experiments in a semi-open system under geological constraint. J Pet Sci Eng 2021;201:108412.
[36] Rubinstein I, Spyckerelle C, Strausz OP. Pyrolysis of asphaltenes: a source of geochemical information. Geochim Cosmochim Acta 1979;43(1):1–6.
[37] Xiong Y, Geng A. Carbon isotopic composition of individual n-alkanes in asphaltene pyrolysates of biodegraded crude oils from the Liaohe Basin, China. Org Geochem 2000;31(12):1441–9.
[38] Shock EL, Canovas P, Yang Z, Boyer G, Johnson K, Robinson K, et al. Thermodynamics of organic transformations in hydrothermal fluids. Rev Mineral Geochem 2013;76(1):311–50.
[39] Dick JM, Evans KA, Holman AI, Jaraula CMB, Grice K. Estimation and application of the thermodynamic properties of aqueous phenanthrene and isomers of methylphenanthrene at high temperature. Geochim Cosmochim Acta 2013;122:247–66.
[40] Seewald JS. Evidence for metastable equilibrium between hydrocarbons under hydrothermal conditions. Nature 1994;370(6487):285–7.
[41] Seewald JS. Aqueous geochemistry of low molecular weight hydrocarbons at elevated temperatures and pressures: constraints from mineral buffered laboratory experiments. Geochim Cosmochim Acta 2001;65(10):1641–64.
[42] Peters KE, Walters CC, Moldowan JM. The Biomarker Guide: Volume 2: Biomarkers and Isotopes. In: Petroleum Systems and Earth History. 2 ed. Cambridge: Cambridge University Press; 2004.
[43] Berwick LJ, Greenwood PF, Meredith W, Snape CE, Talbot HM. Comparison of microscale sealed vessel pyrolysis (MSSVpy) and hydropyrolysis (Hypy) for the characterisation of extant and sedimentary organic matter. J Anal Appl Pyrol 2010;87(1):108–16.
[44] Gürgey K. Geochemical effects of asphaltene separation procedures: changes in sterane, terpane, and methylalkane distributions in maltenes and asphaltene co-precipitates. Org Geochem 1998;29(5):1139–47.
[45] Xiao H, Li M, Yang Z, Zhu Z. Distribution patterns and geochemical implications of C19–C23 tricyclic terpanes in source rocks and crude oils occuring in various depositional environments. Acta Geochimica 2019;48(2):161–70. in Chinese.
[46] Philp P, Symcox C, Wood M, Nguyen T, Wang H, Kim D. Possible explanations for the predominance of tricyclic terpanes over pentacyclic terpanes in oils and rock extracts. Org Geochem 2021;155:104220.
[47] Wang T-G, Li M, Wang C, Wang G, Zhang W, Shi Q, et al. Organic molecular evidence in the Late Neoproterozoic Tillites for a palaeo-oceanic environment during the snowball Earth era in the Yangtze region, southern China. Precambrian Res 2008;162(3-4):317–26.
[48] Zhao W, Wang X, Hu S, Zhang S, Wang H, Guan S, et al. Hydrocarbon generation characteristics and exploration prospects of Proterozoic source rocks in China. Sci China Earth Sci 2019;62(6):909–34.
[49] Mackenzie AS, Brassell SC, Eglinton G, Maxwell JR. Chemical fossils: the geological fate of steroids. Science 1982;217(4559):491–504.
[50] Moldowan JM, Fago FJ. Structure and significance of a novel rearranged monoaromatic steroid hydrocarbon in petroleum. Geochim Cosmochim Acta 1986;50(3):343–51.
[51] Moldowan JM, Fago FJ, Carlson RMK, Young DC, an Duvne G, Clardy J, et al. Rearranged hopanes in sediments and petroleum. Geochim Cosmochim Acta 1991;55(11):3333–53.
[52] Zhu Y, Xiao Q. The effect of oxidation-reduction nature of despositional environments on the formation of diasteranes. Acta Sedimentologica Sinica 1997;15(4):103–8. in Chinese.
[53] Jin X, Zhang Z, Wu J, Zhang C, He Y, Cao L, et al. Origin and geochemical implication of relatively high abundance of 17α (H)-diahopane in Yabulai basin, northwest China. Mar Pet Geol 2019;99:429–42.
[54] Fang P, Wu J, Li B, Cheng B, Song D, Zhong N. Nondestructive investigation on hydrocarbons occluded in asphaltene matrix: The evidence from the dispersive solid-phase extraction. J Pet Sci Eng 2022:110890.